Thermo-structural Behavior in a Series of Lanthanide-Containing Polyoxotungstate Hybrids with Copper(II) Complexes of the Tetraazamacrocycle Cyclam: a Single-Crystal-to-Single-Crystal Transformation Study

Jagoba Martín–Caballero,[†] Beñat Artetxe,[‡] Santiago Reinoso,[§] Leire San Felices,[‖] Pablo Vitoria,[‡] Aitor Larrañaga,[‖] José Luis Vilas[*,†,⊥] and Juan M. Gutiérrez–Zorrilla[*,†,‡]

[†]BCMaterials, Basque Center for Materials, Applications and Nanostructures, UPV/EHU Science Park, 48940 Leioa, Spain.

[‡]Departamento de Química Inorgánica, Facultad de Ciencia y Tecnología, Universidad del País Vasco UPV/EHU, P.O. Box 644, 48080 Bilbao, Spain.

[§]Institute for Advanced Materials (InaMat), Universidad Pública de Navarra (UPNA), Edificio Jerónimo de Ayanz, Campus de Arrosadia, 31006 Pamplona, Spain.

[‖]Servicios Generales de Investigación SGIker, Facultad de Ciencia y Tecnología, Universidad del País Vasco UPV/EHU, P.O. Box 644, 48080 Bilbao, Spain.

[⊥]Departamento de Química Física, Facultad de Ciencia y Tecnología, Universidad del País Vasco UPV/EHU, P.O. Box 644, 48080 Bilbao, Spain.

Supporting Information Placeholder

ABSTRACT: The series of fourteen isostructural $[Cu(cyclam)]_2[\{Cu(cyclam)\}_4\{(\alpha\text{–}GeW_{11}O_{39})Ln(H_2O)(OAc)\}_2]\cdot 18H_2O$ (**1–Ln**, Ln = La to Lu; cyclam = 1,4,8,11–tetraazacyclotetradecane) polyoxometalate-based hybrids reported herein represent: (i) the first example of a 2-dimensional covalent hybrid lattice involving the $[\{(\alpha\text{–}XW_{11}O_{39})Ln(H_2O)(OAc)\}_2]^{n-}$ archetype; and (ii) the first structural characterization of such dimeric polyoxotungste for Ln = La and Pr, as well as for the combination of X = Ge and Ln = Ce, Nd, Sm or Lu. Compounds **1–Ln** have been characterized by elemental analyses, infrared spectroscopy and thermogravimetry, and their thermo–structural behavior has been monitored by powder and single-crystal X-ray diffraction. The title compounds undergo two single–crystal–to–single–crystal transformations triggered by thermal dehydration to lead to the $[\{Cu(cyclam)\}_6\{(\alpha\text{–}GeW_{11}O_{39})Ln(H_2O)(OAc)\}_2]\cdot 4H_2O$ intermediate (**2–Ln**, Ln = Eu, Er) and $[Cu(cyclam)]_{0.5}[\{Cu(cyclam)\}_{5.5}\{(\alpha\text{–}GeW_{11}O_{39})Ln(OAc)\}_2]$ (**3–Ln**, Ln = Ce, Eu) final anhydrous phases, the latter evidencing a coordinatively unsaturated derivative of the dimeric archetype for the first time. These transitions involve formation and disruption of $Cu\text{–}O_{POM}$ bonds that result in different $\{Cu(cyclam)\}^{2+}$ moieties grafting at and releasing from Keggin surfaces, which reduces the dimensionality of **1–Ln** to 1-dimensional covalent assemblies for **2–Ln** and **3–Ln**. While all **3–Ln** phases rehydrate fully upon exposure to air for 24 h, the kinetics governing the crystal transitions back toward **1–Ln** through **2–Ln** depend on the nature of Ln. Under ambient moisture, the anhydrous structures fully revert back to the parent framework for Ln = La–to–Sm, while the Eu–to–Lu–containing samples afford mixtures of **1–Ln** and **2–Ln** and require immersion in water for the structural reversion to be completed. Single-crystal X-ray diffraction analyses on the rehydrated **1R–Ln** samples (Ln = Ce, Eu and Er) support these observations.

INTRODUCTION

Single–crystal–to–single–crystal (SCSC) transformations of crystalline materials constitute a relevant phenomenon within the crystal engineering or the solid–state and supramolecular chemistries, hence within the materials science.[1–4] For coordination compounds, disruption and formation of metal-to-ligand bonds is often observed in the course of such transformations, and this fact can result in dramatic structural modifications that can in turn promote changes in e.g. the magnetic, catalytic or sorption properties.[5–9] The occurrence of SCSC transitions allows the exact monitoring of how the location of atoms and molecules change within the structure after a given external stimulus (e.g. heat, light, ion–exchange, etc.) is applied to the crystalline materials, and therefore, it provides detailed structural information about the transition mechanisms and their relationship with the properties subject of interest.[10–15]

To date, a large number of SCSC transitions have been described for organic[16–19] or coordination[20–25] compounds, but reports on such phenomenon are comparatively uncommon for polyoxometalate (POM)-based structures.[26] Among the latter, thermally triggered transformations are limited to a few examples besides the polymorphic transitions in $[Co(Hbpe)_2(V_4O_{12})]$ (bpe = 1,2-di(4-pyridyl)ethane),[27] $[C(NH_2)_3]_6[Mo_7O_{24}]\cdot H_2O$,[28] and $[Tm_2(H_2O)_{14}(H_6CrMo_6O_{24})]$-$[H_6CrMo_6O_{24}]\cdot 16H_2O$.[29] These examples are associated with the structural response of certain POM-based molecular compounds or extended lattices to the thermal evacuation of guest solvent molecules[30] and they include: the monitoring of the packing compaction in $H_5PV_2Mo_{10}O_{40}\cdot 36H_2O$;[31] the crystal dynamics leading to the collapse of the porous $[Co_4(ppca)_4(H_2O)_2(V_4O_{12})]\cdot 7.2H_2O$ 3-dimensional framework (ppca = 4–(pyridine–4–yl)pyridine–2–carboxylate);[32] the robustness of the porous $Cs_5[Cr_3O(O_2CH)_6(H_2O)_3]$-$[CoW_{12}O_{40}]\cdot 7.5H_2O$ ionic crystal;[33] the reversible grafting of metal-organic subunits at POM surfaces and the ligand conformation changes found in hybrids made of $[\alpha\text{–}XW_{12}O_{40}]^{4-}$ anions (X = Ge, Si) and Cu^{II} complexes of bis(aminopyridyl)–type ligands;[34,35] or the reversible dissociation of dimeric Cu^{II}–picolinate species in $[C(NH_2)_3]_4[\{XW_{12}O_{40}\}\{Cu_2(pic)_4\}]$-$\cdot[Cu_2(pic)_4(H_2O)]_2\cdot 6H_2O$ (X = Ge, Si).[36] We are now exploring the ability of transition-metal (TM) complexes of macrocyclic polyamines to link POMs into open-framework materials analogous to MOF (metal-organic framework) architectures, and how dehydration affects the structure of such POMOF-like materials. We have focused our studies on the complex $[Cu(cyclam)]^{2+}$ and reported a series of 2- or 3-dimensional covalent lattices with isoPOMs such as heptatungstate,[37] metavanadate,[38] decavanadate,[39] and octamolybdate.[40] The former two compounds display dynamic response to thermal dehydration that results in the collapse or modification of the porous structure via consecutive SCSC transitions, whereas the latter two dehydrate with minimal structural effects, the decavanadate-based compound showing features of a robust microporous material.

POMs are a family of anionic metal–oxide clusters with large topological diversity and intrinsic multifunctional nature,[41,42] among which lanthanide(Ln)-containing polyoxotungstates (POTs) constitute one of the most thoroughly studied POM subclasses.[43,44] The $[\{(\alpha\text{–}XW_{11}O_{39})Ln(H_2O)(OAc)\}_2]^{n-}$ archetype is a representative example of Ln–containing POTs, being composed of two Keggin–type monosubstituted units linked into a dimeric entity through acetate (OAc) ligands that bridge the Ln centers in chelating (η^2–μ–1,1) coordination mode. The first two examples of such species were isolated by Mialane et al. in 2004 (X = Si, Ln = Gd, Yb),[45] and the series was later expanded to additional combinations of heteroatoms (X) and Ln ions by Patzke's (X = Ge, Ln = Eu–Yb),[46] Wang's (X = P, Ln = Sm–Er),[47] Hussain's (X = Si, Ln = Eu–Tb),[48] and Niu's groups (X = P, Ln = Dy, Lu).[49] It is worth remarking that POT analogues containing early Ln ions have not been isolated yet as salts of standard cations, and have only been observed in combination with TM-organic moieties as part of hybrid compounds instead. The grafting of such moieties to these POTs has met limited success; literature examples are limited to just five structures, and to our knowledge, they are all based on Cu^{II}–ethylendiamine complexes. These examples include POTs with the following combinations of X and Ln: X = Si and Ln = Ce, Nd, Sm;[50] X = P and Ln = Sm;[51] and X = Ge and Ln = Tb.[51] Among them, that based on the Ce–containing silicotungstate is the only compound showing an extended structural motif, which consists in a ladder–like 1–dimensional covalent assembly. The other four hybrids are discrete POT entities with the complexes grafted at the surface as decorating subunits.

We are now extending our studies on the linking ability of $[Cu(cyclam)]^{2+}$ to POMs other than isoPOMs, and investigating any structural response to dehydration that such hybrid materials could show through SCSC transitions. Here we report the thermo–structural behavior of the series $[Cu(cyclam)]_2[\{Cu(cyclam)\}_4\{(\alpha\text{–}GeW_{11}O_{39})Ln(H_2O)(OAc)\}_2]$-$\cdot 18H_2O$ (**1–Ln**), which represents the first example of a covalent 2-dimensional hybrid network based on the $[\{(\alpha\text{–}XW_{11}O_{39})Ln(H_2O)(OAc)\}_2]^{n-}$ archetype. This series has been isolated for all Ln ions from La to Lu, and therefore, the structural characterization of such POTs with Ln = La and Pr, or with the combination X = Ge and Ln = Ce, Nd, Sm, or Lu is provided for the first time. The title compounds undergo two SCSC transitions triggered by the thermal release of water molecules to give the partially dehydrated intermediates $[\{Cu(cyclam)\}_6\{(\alpha\text{–}GeW_{11}O_{39})Ln(H_2O)(OAc)\}_2]\cdot 4H_2O$ (**2–Ln**) and the final $[Cu(cyclam)]_{0.5}[\{Cu(cyclam)\}_{5.5}\{(\alpha\text{–}GeW_{11}O_{39})Ln(OAc)\}_2]$ anhydrous phases (**3–Ln**). The dimensionality of the parent **1–Ln** lattice is reduced to chain-like assemblies in the **2–Ln** and **3–Ln** phases according to single-crystal X-ray diffraction analyses of the **2-Eu**, **2-Er**, **3-Ce**, and **3-Eu** derivatives. The transitions have been found to be reversible, but with kinetics that depend on the Ln nature.

RESULTS AND DISCUSSION

Synthesis

We have made use of a hydrothermal synthetic approach to isolate the series of fourteen $[Cu(cyclam)]_2[\{Cu(cyclam)\}_4\{(\alpha\text{-}GeW_{11}O_{39})Ln(H_2O)(OAc)\}_2]\cdot 18H_2O$ isostructural compounds (**1–Ln**) that we report herein. This series comprises examples of the $[\{(\alpha\text{–}XW_{11}O_{39})Ln(H_2O)(OAc)\}_2]^{n-}$ archetype for all of the Ln ions from La to Lu. Such dimeric POTs with Ln = La and Pr or with the combination X = Ge and Ln = Ce, Nd, Sm or Lu are unprecedented. The synthesis was accomplished using two different methods (see the Experimental Section in the Supporting Information). Method 1 involves the reaction of the $[\alpha\text{–}GeW_9O_{34}]^{10-}$ precursor, Ln ions and the *in situ* prepared $[Cu(cyclam)]^{2+}$ complex in 1M KOAc/HOAc medium at 160 °C under autogenous pressure for 3 days. This method allowed us accessing the whole **1–Ln** series (Ln = La to Lu) with a common synthetic protocol, and yielded mixtures of polycrystalline powder and plates suitable for single-crystal X-ray diffraction (SCXRD) except for Ln = Eu–Er, for which the powder was the single material isolated. Infrared (FT-IR) spectroscopy and powder X-ray diffraction (PXRD) analyses (Figures S1–S3 and Figure S4 in the Supporting Information) confirmed that the polycrystalline fraction and the plates corresponded to the same phase in all cases. Single crystals of **1–Ln** derivatives with Ln = Eu–Er could be obtained by using $[\{(\alpha\text{–}GeW_{11}O_{39})Ln(OAc)(H_2O)\}_2]^{12-}$ preformed precursors instead of $[\alpha\text{–}GeW_9O_{34}]^{10-}$ and the Ln source under the same synthetic conditions (method 2),

although the yields observed were *ca.* four times lower than those obtained with method 1.

Since compounds **1–Ln** contain $[\alpha\text{–}GeW_{11}O_{39}]^{8-}$ fragments instead of the starting $[\alpha\text{–}GeW_9O_{34}]^{10-}$ subunit, we attempted their preparation using the $K_8[\alpha\text{–}GeW_{11}O_{39}]$ precursor under similar hydrothermal conditions, but these reactions resulted in brown precipitates that did not correspond to **1–Ln** according to PXRD and FT–IR analyses (Figure S5 in the Supporting Information). Analogous results were obtained when starting with a $1GeO_2$:$11Na_2WO_4$ molar mixture or with the $K_4[GeW_{12}O_{40}]$ precursor, which are both expected to lead to $[\alpha\text{–}GeW_{11}O_{39}]^{8-}$ in our buffered medium. These observations suggest that the $[\alpha\text{–}GeW_9O_{34}]^{10-}$ to $[\alpha\text{–}GeW_{11}O_{39}]^{8-}$ transformation is a key step in the formation of the **1–Ln** framework. It is also worth noting that the title series could not be isolated when NaOAc/HOAc buffers or water were used as the reaction media, showing that K^+ ions must also play a key role in the formation of **1–Ln** even if they are absent from the final structure. This conclusion is further supported by the fact that more diluted 0.5 M KOAc/HOAc buffer was neither suitable for preparing compounds **1–Ln**. The isolation of the title series was also found to depend on the nature of TM, and more specifically, on the plasticity of the Cu^{II} coordination sphere, as analogous reactions that involved Co^{II}, Ni^{II} or Zn^{II} ions instead of Cu^{II} did not lead to any crystalline material, but to amorphous precipitates. We also explored whether compounds **1–Ln** could be prepared under bench conditions by applying thermal treatments from room temperature to reflux conditions to the reaction mixtures from both methods 1 and 2. These experiments did not result in the **1–Ln** series, but in a second family of hybrid systems based on $[Ln(\alpha\text{–}GeW_{11}O_{39})_2]^{13-}$ Peacock–Weakley-type POMs instead. The full chemical and thermo-structural characterization of such hybrids is now in progress.

Thermo-Structural Behavior

The thermal stability of the **1–Ln** series was investigated by a combination of thermogravimetric (TGA/DTA) and variable-temperature (VT) PXRD experiments. The TGA/DTA curves of all compounds **1–Ln** show almost identical profiles that follow a dehydration–stability–decomposition sequence in which both the dehydration and decomposition stages are made of several highly overlapping mass losses (Figure S6 in the Supporting Information). Dehydration is observed as two successive mass losses that extend from room temperature to 100–115 °C, and from the corresponding temperature in this range to 165–180 °C. The first loss is relatively steep, associates with a set of at least two endothermic DTA signals centered at T_{min} = 40–50 °C and 75–85 °C, and accounts for 3.68–4.07% of the total mass, which corresponds to the release of 17 water molecules. The second loss (0.56–0.80%) is significantly more subtle, originates from a single endothermic process centered at T_{min} ≈ 140 °C, and involves the release of 3 additional water molecules. The resulting anhydrous phases show noticeable range of thermal stability that becomes wider as the Ln ion varies from Ce to Lu. This fact is due to the upper limit temperature before decomposition increasing with the Ln atomic number, from ca. 230°C for **1–Ln** derivatives with the lighter La–Pr atoms to ca. 260 °C for those phases with the heaviest metal ions Yb and Lu. Thermal decomposition takes place via three highly overlapping mass losses of exothermic nature as indicated by the collection of DTA signals centered at T_{max} ≈ 325, 460 and 575 °C. These processes result from the combustion of the OAc and cyclam ligands combined with the breakdown of the Keggin-type framework. The mass loss for the decomposition stage ranges from 16.39 to 17.01%, and these values are in all cases consistent with those calculated for six cyclam and two OAc ligands (16.82–16.97%). The final residues are obtained at temperatures above 610 °C and they account for 78.6–79.1% of the total mass, which compare well with the values calculated for solid $Cu_6Ge_2Ln_2O_{78}W_{22}$ mixtures (ca. 78.5%).

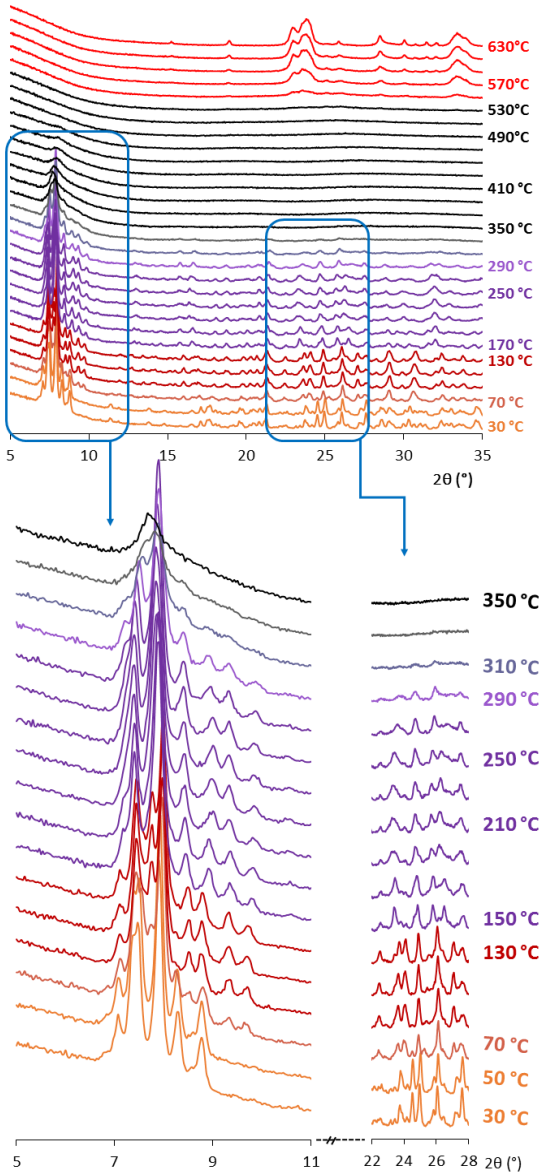

Figure 1. VT-PXRD patterns for **1-Er** from 30 to 630°C.

The experimental PXRD patterns of compounds **1–Ln** (Figure S7 in the Supporting Information) are consistent with those simulated from SCXRD data, which confirms the **1–Ln** samples as single and homogeneous crystal phases; suggests a good phase purity; and makes them suitable for further VT-PXRD experiments to explore whether they retain crystallinity upon dehydration, and in such case, whether they show robust nature for which solvent molecules are evacuated

without structural impact or dynamic behavior involving crystal transitions as structural response. Figure 1 shows the VT-PXRD patterns of **1–Er** to exemplify the thermo-structural behavior of the title compounds. Figure S8 in the Supporting Information gathers the VT-PXRD patterns for the remaining 13 **1–Ln** derivatives, while Figures S9 and S10 display those of **1–Ce** and **1–Eu** in more detail.

Compound **1–Er** retains full crystallinity throughout the whole dehydration process and subsequent stage of thermal stability up to a temperature in the 270–290 °C range, which compares well with that determined from the TGA curve. For comparison, the upper limit temperatures for those phases that contain early- (**1–Ce**) or mid- (**1–Eu**) Ln ions instead of a late Ln ion such as Er lie in the ranges 230–250 °C and 250–270 °C, respectively. This result is consistent with the observation in the TGA curves of the upper limit temperature of the stability range increasing with the Ln atomic number. At higher temperatures corresponding to the decomposition stage in the TGA curve, the diffraction maxima start broadening and losing intensity progressively until they fade away at temperatures that range from ca. 310 °C for **1–Ce** to ca. 350 °C for **1–Eu** and ca. 410 °C for **1–Er**. The resulting solids maintain the amorphous character up to temperatures about 490–530 °C, above which new crystal phases corresponding to the final residue of the thermal decomposition start forming. At *ca.* 610 °C, these phases can be identified as mixtures of tetragonal $P4/nmm$ WO_3 (PDF: 01–085–0807),[52] and triclinic $P\bar{1}$ $CuWO_4$ (PDF: 01–088–0269[53] for **1–Ce**, 01–080–1918[54] for **1–Eu**, or 01–070–1732[55] for **1–Er**) as shown in Figure S11 in the Supporting Information. We could not identify any Ln-containing phase from these diffraction patterns. This fact could be attributed to such phases being of amorphous character, but it could also be due to the Ln ions doping the $CuWO_4$ scheelite instead of forming a separate phase upon considering that lanthanide tungstates are known to display the so-called defective-scheelite-type structure.[56]

Close inspection of the low-temperature region of crystallinity reveals low-to-moderate thermal stability for the **1–Ln** framework as its diffraction pattern is kept unaltered only up to 50 °C. At 70 °C, significant modifications in both positions and heights are observed for the collection of diffraction maxima of weak intensity located at 2θ values in the ranges 8–10° and 22–28°, including the appearance of new, additional peaks. This behavior is indicative of the system transitioning to a second crystalline phase, which appears to be fully formed at 90 °C and remains stable up to temperatures in the 130–150 °C range. At higher temperatures near those corresponding to the release of all water molecules as estimated from the TGA curves, a second crystal transition takes place according to further variations in the 2θ ranges selected to monitor the diffraction patterns. Therefore, our studies confirm compounds **1–Ln** as dynamic systems with a structural response to thermal dehydration that involves two sequential crystal transitions into a partially dehydrated intermediate **2–Ln** and a final anhydrous phase **3–Ln**.

Crystal structure of compounds 1-Ln

Compounds **1–Ln** are all isostructural (Table S1 in the Supporting Information). They crystallize in the triclinic space group $P\bar{1}$ with an asymmetric unit that contains one half of a $[\{(\alpha\text{–}GeW_{11}O_{39})Ln(H_2O)(OAc)\}_2]^{12-}$ anion, four cationic $\{Cu(cyclam)\}^{2+}$ moieties (Cu1A/Cu1D in general positions, and Cu1B/Cu1C located on centers of inversion) and 9 water molecules of hydration (of which 3 disordered). Figure 2 shows the ORTEP view of **1–Eu** as a representative example of the whole **1–Ln** series.

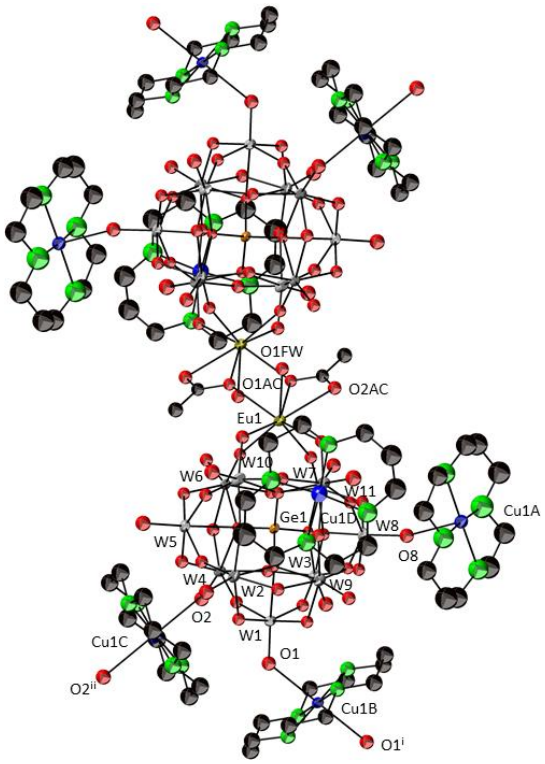

Figure 2. ORTEP view of **1–Eu** with atom labelling (50% probability level; water molecules of hydration and H atoms are omitted for clarity). Symmetry codes: i) 1+*x*, 1+*y*, 1+*z*; ii) *x*, *y*, 1+*z*.

The Ln coordination sphere is defined by the four O atoms that delimit the vacant site of one monolacunary Keggin-type cluster, two O atoms from a bridging OAc ligand, another O atom from the centrosymmetrically-related OAc ligand and one terminal water molecule. The Ln–O bonding scheme (Table S2 in the Supporting Information) includes four shorter bonds with the O_{POM} atoms and four longer bonds with the capping OAc and terminal aqua ligands, which are similar in length. Figure S12 in the Supporting Information evidences that the length of the Ln–O_{POM}, Ln–O_{Ac} and Ln–O_w bonds, as well as the Ln···Ln distance within the dimeric POT, decrease linearly by 0.2–0.3 Å with the increase of the Ln atomic number due to the well-known Ln contraction effect.[57,58] In contrast, the Ln–O bond involving the centrosymmetrically-related OAc ligand is not influenced by this effect according to its random variation in length along the series. The coordination geometry is highly distorted as shown by the Continuous Shape Measures (CShM)[59] obtained when comparing the experimental LnO_8 polyhedra with all possible 8–coordinated ideal shapes, the values of which are significantly higher than one. The biaugmented trigonal prism (BTPR) and square antiprism (SAPR) afford comparable CShM values that are much lower than those of any other shape (Table S3 in the Supporting Information),

hence the LnO_8 polyhedra can be best described as intermediate between both BTPR and SPAR geometries, being closer to the former for the lighter Ln ions (La, Ce) and progressively becoming more similar to the latter as the Ln atomic number increases.

Different coordination geometries associated with different structural roles are found among the $\{Cu(cyclam)\}^{2+}$ moieties. Each Keggin unit displays three of such moieties grafted at the POM surface: Cu1A, Cu1B and Cu1C. Cu1A is a surface-appended antenna unit in which the Cu^{II} center shows elongated CuN_4O square–pyramidal geometry with the four N atoms of the cyclam ligand in the basal plane and a terminal O_{POM} atom in the apical position. In contrast, both Cu1B and Cu1C act as linking moieties by adopting distorted octahedral geometries with the cyclam ligand in the equatorial plane and terminal O atoms from two centrosymmetrically-related Keggin units of neighboring dimeric POTs in the axial positions. The fourth moiety, Cu1D, is a non–supported complex with square-planar coordination geometry, the structural role of which is to act as charge-balancing cation. Table S4 in the Supporting Information shows that the Cu–O_{POM} bonds are not affected by the Ln contraction effect according to their subtle variations along the series (ca. 0.05 Å), and that the Jahn–Teller elongation shown by the CuN_4O_2 chromophores of Cu1B and Cu1C is especially remarkable for the latter, as its axial bonds show lengths near those of semi–coordination. Regardless of the coordination geometries, all moieties display the so–called *trans–III* configuration in which the N–H bonds of the two pairs of propylene-bridged N atoms point at opposite directions with respect to the CuN_4 plane.[60] According to DFT calculations, this configuration is the most favorable for octahedral geometries among the five different geometrical isomers that the TM(cyclam) complexes can adopt depending on the ligand conformation (Figure S13 in the Supporting Information).[61] These studies have also shown that the *trans–I* configuration gains stability over the *trans–III* for tetracoordinated TM centers, but in our case, the Cu1D square–planar complex retains the latter isomeric form, which might be associated with packing effects. In fact, we have always observed the *trans–III* form in all of our previous POM–Cu(cyclam) hybrid systems.[37–40]

The crystal packing of compounds **1–Ln** displays intrinsic layered nature and contains covalent 2–dimensional hybrid assemblies parallel to the (1–10) plane in which each dimeric POT is linked to four neighboring analogues along the [111] and [001] directions through the Cu1B and Cu1C moieties, respectively. Such connectivity follows a staggered brickwork grid pattern with rectangular intralamellar cavities of dimensions about 7.9 × 23.0 Å (Figure 3). This assembly constitutes the first example of a 2-dimensional covalent hybrid network based on the $[\{(\alpha\text{–}XW_{11}O_{39})Ln(H_2O)(OAc)\}_2]^{n-}$ archetype. The hybrid layers stack with the Cu1A antenna units oriented toward the interlamellar space, where the charge-balancing Cu1D cations are also located. These moieties are tilted with respect to the mean plane of the hybrid layers and their cyclam ligands point at the rectangular grid cavities. This fact, together with the offset of the stacking, precludes the formation of channels hosting the guest water molecules along the stacking direction as observed for some of our previous POM–Cu(cyclam) systems.[37,39] However, the solvent accessible space is not fully blocked in the **1–Ln** framework, which is intersected by zigzagging channels along the crystallographic *b* axis and by strings of discrete compartments parallel to the [100] direction (Figure S14 in the Supporting Information). PLATON[62] analyses reveal that the solvent accessible volume is ca. 18% of the unit cell and distributes as follows: 12% associates with the zigzagging channels and two discrete compartments account for 3% each.

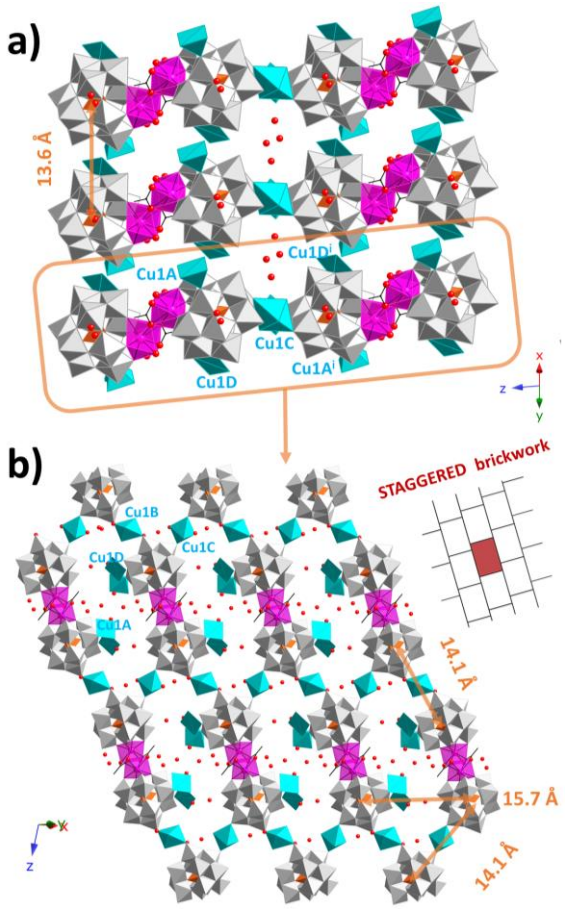

Figure 3. a) Crystal packing of **1–Ln** along the [110] direction (cyclam ligands are omitted for clarity). b) Projection of a hybrid covalent layer in the (1–10) plane.

Sequential SCSC Transformations

To get further insight into the crystal dynamics that the **1-Ln** framework undergoes with thermal dehydration, we carried out variable-temperature SCXRD studies (VT-SCXRD) to determine the structures of the partially dehydrated intermediate and final anhydrous phases. We selected three representative examples out of the fourteen isostructural compounds to illustrate the phase transitions of **1-Ln** frameworks containing early- (**1–Ce**), mid- (**1–Eu**) and late- (**1–Er**) Ln ions. These compounds were chosen because of the higher diffraction quality of their crystals, which maintained their integrity without any noticeable cracking and preserved their single-crystal diffracting nature during the whole routine.

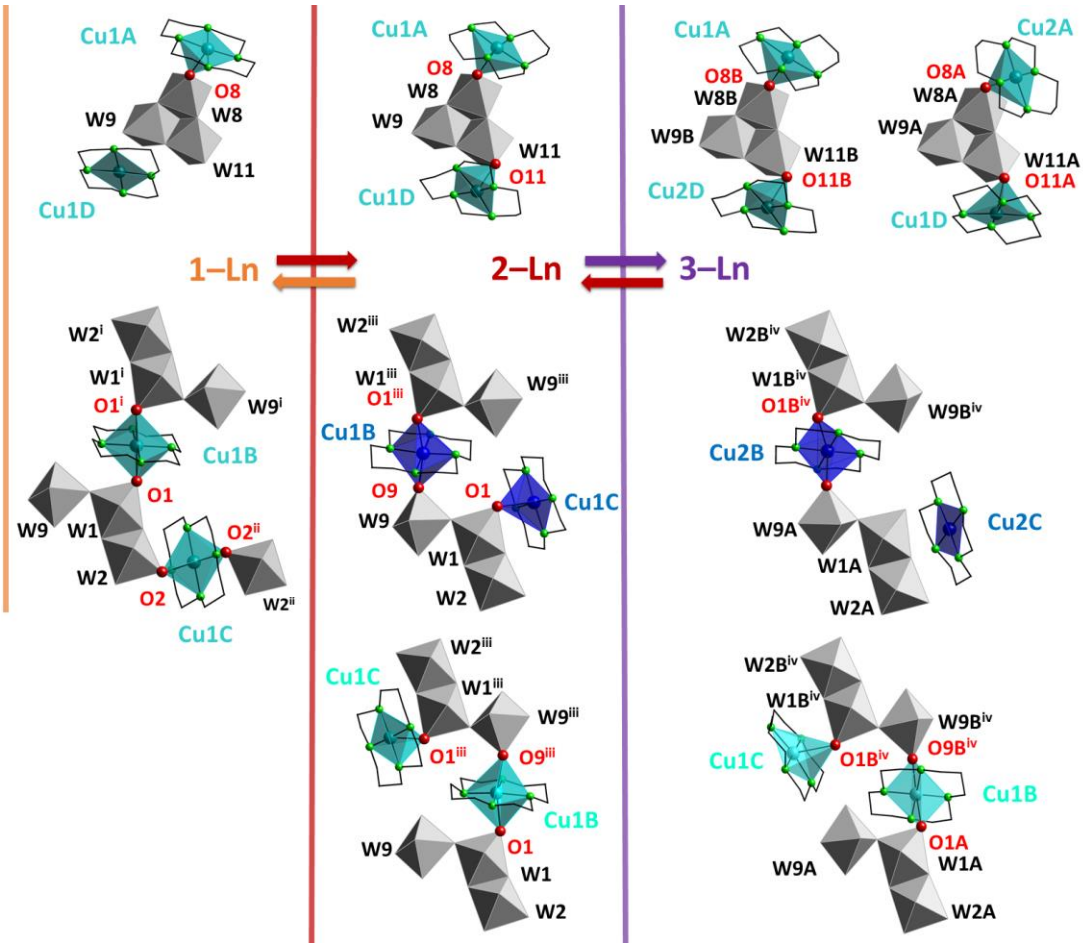

Figure 4. Evolution of the Cu–O_{POM} bonding scheme for the different $\{Cu(cyclam)\}^{2+}$ moieties found in the parent **1–Ln** framework throughout the two sequential SCSC transformations into the partially dehydrated **2–Ln** intermediate and the final anhydrous **3–Ln** derivative. The Cu atoms belonging to the two different packing forms originating from the crystallographic disorder observed in **2–Ln** and **3–Ln** are depicted in different tones of blue. Symmetry codes: i) $-x, -1-y, 1-z$; ii) $1-x, -y, 1-z$, iii) $-x, -y, 1-z$, iv) $x, y, 1+z$.

We could determine the structures of the isostructural **2-Eu** and **2-Er** intermediates, as well as those of the isostructural **3-Ce** and **3-Eu** anhydrous phases. Unfortunately, we failed in determining those of **2-Ce** and **3-Er** due to these phases, the existence of which is unequivocally confirmed by VT-PXRD, undergoing fast rehydration. Crystals of the Er-derivative heated to 160 °C repeatedly afforded the parameters corresponding to **2-Er** instead of those expected for the anhydrous phase, and so did the Tm-to-Lu-containing analogues, which confirmed the impossibility of determining the structure of **3-Ln** for those frameworks containing late-Ln ions. Analogously, the attempts of determining the structure of **2-Ce** always afforded the unit cell parameters of **1-Ce**; hence those frameworks containing mid-Ln ions such as Eu stood out as the only examples within the series able to lead to partially dehydrated and anhydrous structures that are stable enough toward moisture for being inspected by SCXRD analyses.

Transformation of 1-Ln into 2-Ln. The **2–Ln** intermediates also crystallize in the triclinic *P*–1 space group with a shortening of the parameter *a* by ca. 0.6 Å and a slighter lengthening of *c*, which results in a smaller unit cell volume indicative of a more compact crystal architecture (Table S1 in the Supporting Information). Besides two localized water molecules of hydration, the unit cells also contain one half of a $[\{(\alpha\text{–}GeW_{11}O_{39})Ln(H_2O)(OAc)\}_2]^{12-}$ anion and four crystallographically independent $\{Cu(cyclam)\}^{2+}$ moieties, but Cu1B and Cu1C are now shifted from centers of inversion toward general positions and display half occupancies.

Partial dehydration brings forth drastic changes in the crystal packing of the **2–Ln** phases, which include significant modifications in the Cu–O_{POM} bonding scheme and the dimensionality of the hybrid framework. The most remarkable change consists in the generation of crystallographic disorder involving the Cu1B and Cu1C moieties, which results in the two packing forms that are represented in Figure 4. The Cu1C moiety migrates from being coordinated at two centrosymmetrically-related W2 octahedra in **1–Ln** to grafting at the adjacent W1 site of the same $\{W_3O_{13}\}$ trimer in the structure of **2–Ln**, thus losing its bridging character and becoming a square-pyramidal antenna moiety as a result of the disruption of one of its Cu–O_{POM} bonds. The Cu1B moiety retains its parent geometry and linking character, but the migration of Cu1C forces one of its two centrosymmetrically-related W1 anchoring sites in **1–Ln** to be displaced toward the neighboring corner-sharing W9 octahedron in **2–Ln**. The Cu1D moiety, which acted as a square-planar cation located in the vicin-

ity of the W9 octahedron in **1–Ln**, grafts in turn at the adjacent edge-sharing W11 site to become the third type of square-pyramidal antenna moiety that decorates the surface of the Keggin units in **2–Ln** besides Cu1C and Cu1A, the latter representing the single moiety that remains unaffected by the SCSC transition but for a shortening of its apical Cu–O_{POM} bond (Table S5 in the Supporting Information).

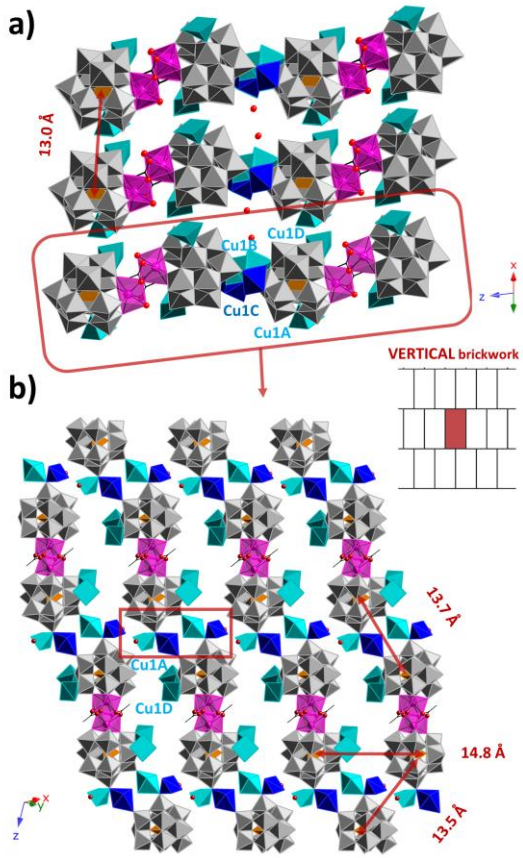

Figure 5. a) Crystal packing of **2–Ln** along the [110] direction (cyclam ligands are omitted for clarity). b) Projection of a hybrid supramolecular layer in the (1–10) plane. Color code: same as in Figures 3 and 4.

These modifications in the Cu–O_{POM} bonding scheme result in the dimensionality of the hybrid architecture being reduced from the 2-dimensional covalent lattice in **1–Ln** to the 1-dimensional covalent assemblies made of alternating penta-decorated dimeric POTs and $\{Cu(cyclam)\}^{2+}$ linking moieties that undulate along the [111] direction in the structure of the **2–Ln** intermediates (Figure 5). Such hybrid chains still arrange in parallel fashion in the (1–10) plane to form supramolecular layers with vertical brickwork pattern as opposed to the staggered pattern found for the covalent grids of **1–Ln**. This pattern change originates from the in-plane rotation by ca. 20° of the dimeric POTs around the axis along which the layers stack (Figure S15 in the Supporting Information), and it is accompanied by significant lamellar compaction that nearly collapses the accessible space in the intralamellar cavities. Taking the Eu-containing series as example, this lamellar compaction clearly reflects in the Ge···Ge distances: that between equivalent Keggin-type units from adjacent chains in **2–Eu** is substantially shorter than the analogous distance along the [110] direction in the covalent grids of **1–Eu** (14.772(3) vs. 15.6975(14) Å), while that between contiguous clusters linked by Cu1B moieties along the [111] direction shortens also from 14.0650(14) in the **1–Eu** grids to 13.742(3) Å in the **2–Eu** chains. The packing undergoes also compaction along the stacking direction as the interlamellar distance between the nearest Keggin-type units shortens from 13.5581(14) to 12.9782(14) Å when going from **1–Eu** to **2–Eu**.

Transformation of 2-Ln into 3-Ln. The SCSC transition of **2–Ln** into **3–Ln** proceeds with retention of the unit cell setting (triclinic *P*–1 space group) and dimensions (*a* and *c*) but for a loss of symmetry elements that almost doubles the parameter *b*, hence the unit cell volume (Table S1 in the Supporting Information). The content of the unit cell is thus doubled with respect to that of the parent **1–Ln** framework and **2–Ln** intermediate, and now shows one anion $[\{(\alpha\text{–}GeW_{11}O_{39})Ln(OAc)\}_2]^{12-}$ (the two $\{(GeW_{11}O_{39})Ln(OAc)\}^{6-}$ fragments of which are labeled as A and B) and eight crystallographically independent $\{Cu(cyclam)\}^{2+}$ moieties in general positions (Cu1A–Cu1D associated with fragment A and Cu2A–Cu2D associated with fragment B), among which the Cu1B/Cu1C pair and their analogues Cu2B/Cu2C show half occupancies and are involved in a crystallographic disorder that resembles that found for the **2–Ln** phases.

Full dehydration involves the release of the aqua ligand O1W from the Ln coordination sphere. The Ln ions, which displayed a LnO_8 geometry intermediate between BTPR and SAPR in **1–Ln** that evolved into a more regular polyhedron with unequivocal BTPR character in **2–Ln** (CShM values of 1.218 (BTPR) and 2.776 (SAPR) for **2–Eu**), thus become 7-coordinated in **3–Ln** (Figure S16 in the Supporting Information) with somewhat shorter Ln–O_{POM} and longer Ln–O_{OAc} bonds compared to the parent framework (Table S2 in the Supporting Information). The highly distorted geometry is best described as capped trigonal prismatic (CShM values of 2.386 and 2.690 for **3–Eu** that are at least one unit lower than those obtained using any other ideal LnO_7 polyhedron as reference shape, see Table S3 in the Supporting Information). Compounds **3–Ce** and **3–Eu** constitute the first coordinatively unsaturated example of the archetype $[\{(\alpha\text{–}XW_{11}O_{39})Ln(H_2O)(OAc)\}_2]^{n-}$ and demonstrate that the aqua ligands can be thermally evacuated from such species to create vacant sites in the vicinity of the Ln centers without affecting the dimeric POT skeleton.

The architecture of **3–Ln** is highly reminiscent of that described for **2–Ln** (Figure 6). The crystal packing still consists in supramolecular hybrid layers stacked along the [1–10] direction and made of 1-dimensional covalent assemblies of coordinatively unsaturated POTs and $\{Cu(cyclam)\}^{2+}$ linkers that undulate along the crystallographic *z* axis in this case. The representative Ge···Ge distances are kept nearly intact upon the SCSC transition of **2–Ln** into **3–Ln**, which evidences that the packing does not undergo further compaction (Figure S15 in the Supporting Information). The moieties Cu1A, Cu1B and Cu1D (and their Cu2A, Cu2B and Cu2D analogues) do not undergo major modifications either, and they retain their structural roles, coordination geometries, grafting sites and Cu–O_{POM} bond lengths (except for the B-type units, see Table S5 in the Supporting Information).

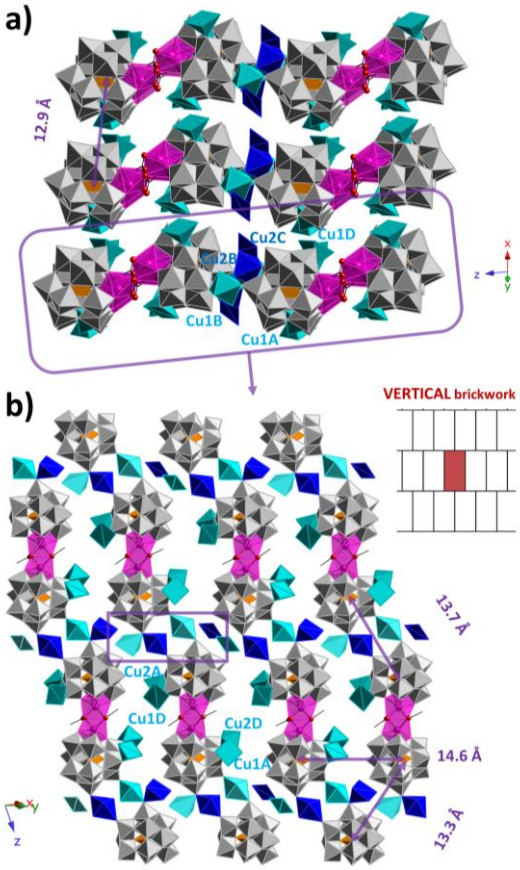

Figure 6. a) Crystal packing of **3–Ln** along the [110] direction (cyclam ligands are omitted for clarity). b) Projection of a hybrid supramolecular layer in the (1–10) plane. Color code: same as in Figures 3 and 4.

In contrast, significant changes are observed for the pair Cu1C/Cu2C, which are involved in crystallographic disorder with the B-type moieties. In this disorder, Cu1B and Cu2B cannot coexist, hence the dimeric POTs are bridged by a single $\{Cu(cyclam)\}^{2+}$ linker in the hybrid chains of **3–Ln**. The coexistence within the Cu1C/Cu2B and Cu1B/Cu2C pairs is neither possible because their organic ligands would overlap. Therefore, Cu1B and Cu2B can only coexist with Cu1C and Cu2C, respectively, which results in two packing forms in the structure of **3–Ln** (Figure 4). The form that contains Cu1B and Cu1C is analogous to those found for **2–Ln** but for a lengthening of the Cu–O_{POM} bonds that is particularly remarkable for the antenna moiety Cu1C, the apical bond of which reaches lengths near those of semicoordination. In the second form, the Cu–O_{POM} bonds of the Cu2B linker are conversely shortened when compared to **2–Ln**, whereas the remaining Cu2C moiety stands out as a square-planar charge-compensating complex with no coordinative interaction with any POT surface (Table S5 in the Supporting Information) instead of remaining in the square-pyramidal antenna role that played in the packing of **2–Ln**. As a result of such disorder, the hybrid chains of **3–Ln** can show three different types of assembly: i) penta-decorated dimeric POTs connected by Cu1B linkers; ii) tetra-decorated dimeric POTs connected by Cu2B linkers; and iii) alternating penta- and tetra-decorated POTs connected by alternating Cu1B and Cu2B linkers. PLATON calculations indicate that our structural solution for **3–Ln** is compact with marginal void spaces, but the anhydrous phases must display some kind of permanent porosity because such structural solution involves disordered $\{Cu(cyclam)\}^{2+}$ moieties that cannot coexist in the crystal packing. The possibility of three different types of 1-dimensional covalent assemblies being present in the structure makes however impossible to discern any accurate extended system of solvent accessible spaces, which prevented us from performing further gas sorption experiments to characterize the porous nature of the **3–Ln** phases.

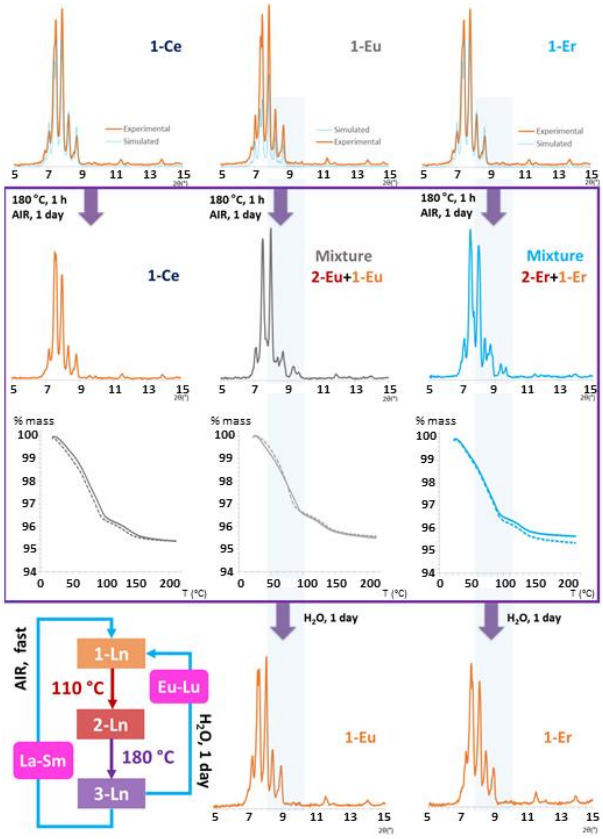

Figure 8. Monitoring of the reversibility of the SCSC transitions that **1–Ce**, **1–Eu** and **1–Er** undergo with thermal dehydration by a combination of PXRD and TGA (continuous line: **3–Ln** exposed to ambient moisture for 24 h; dashed line: **1–Ln**)

Reversibility of the SCSC Transformations. The reversibility of the two SCSC transitions that the **1–Ln** framework undergoes with thermal dehydration has been explored by SCXRD, PXRD and TGA. Figure 8 shows the results obtained for **1–Ce**, **1–Eu** and **1–Er** as representative examples of compounds with early-, mid- and late-Ln ions. The results afforded by the remaining **1-Ln** compounds are compiled in Figure S17 in the Supporting Information. To check whether the **3–Ln** phases were able to absorb water from ambient moisture, and in such case, to determine the extent of the water uptake and whether it was accompanied by any phase transition, freshly prepared **3–Ln** samples were kept in contact with room atmosphere for 24 h before being analyzed by TGA and PXRD. All of the samples were able to undergo water uptake under these conditions and the amount of water absorbed

was ca. 4.5% of the total mass, which accounts well for the 20 water molecules per dimeric POT determined for the parent compounds **1–Ln**. In fact, the shape of the TGA curves recorded up to 215 °C for these samples matches very closely that found for the dehydration stage of the corresponding **1–Ln** phase in all of the fourteen cases analyzed.

While rehydration proved to be feasible and to proceed to completion rapidly without the need of any vapor-saturated environment regardless of the phase composition, the reversibility of the SCSC transitions was found to depend on the specific nature of Ln. For the early–Ln-containing derivatives (Ln = La to Sm), the diffraction patterns collected on **3–Ln** samples exposed to ambient moisture for 24 h were virtually identical to those of **1–Ln**, hence the covalent chains in the anhydrous phases assemble back into the covalent layers of the parent **1–Ln** framework. This reassembly must then involve full reversion of the formation/disruption processes affecting the Cu–O_{POM} bonds and consequent order/disorder transitions involving the $\{Cu(cyclam)\}^{2+}$ moieties. This fact was confirmed by SCXRD analyses on the Ce-containing sample (**1R–Ce**), which showed the unit cell parameters of **1–Ce** (Table S6 in the Supporting Information) and afforded the same architecture with ordered $\{Cu(cyclam)\}^{2+}$ moieties back in their original structural roles, aqua ligands coordinated to Ln ions and most of the hydration water molecules located at their original sites. The full structural solution of **1R–Ce**, together with those of **1R–Eu** and **1R–Er**, are provided as Supporting Information for comparison. In contrast, the PXRD patterns of samples containing mid–to–late Ln ions (Ln = Eu to Lu) displayed diffraction maxima belonging to both the parent **1–Ln** and intermediate **2–Ln** phases, hence the reassembly of hybrid chains into covalent layers could not proceed to completion despite the water uptake by the bulk material indicating full rehydration. These PXRD patterns remained virtually unmodified for samples with long exposures to ambient moisture (up to 2 weeks) and could only be transformed back into those of pristine **1–Ln** phases after soaking such samples in water for 24 h. SCXRD analyses on the soaked Eu- and Er-containing crystals (**1R–Eu** and **1R–Er**) confirm that the structure is transformed back into the parent framework under such conditions.

In view of these results and what observed in the VT-SCXRD experiments, we hypothesize that the kinetics governing the phase transitions from **3–Ln** to **1–Ln** through the **2–Ln** intermediate differ significantly among them and as a function of the Ln ion. For late-Ln ions, the transition from **3–Ln** to **2–Ln** must be very fast as we were unable to determine the anhydrous phase structure of any Er-to-Lu-containing derivative by SCXRD, whereas that from **2–Ln** to **1–Ln** proved to be very slow and could not be fully completed in weeks according to PXRD studies. For early-Ln ions in turn, the transition from **3–Ln** to **2–Ln** must be much slower according to the fact that we could determine the structure of **3–Ce** from SCXRD analyses, whereas that from **2–Ln** to **1–Ln** proved to be as fast as to prevent us from inspecting the SCXRD structure of the intermediate phase. Mid-Ln-containing compounds, such as **1–Eu**, must represent an intermediate situation in which the kinetics of the two SCSC transformations are slow enough for the structures of both the anhydrous and intermediate phases to be inspected by SCXRD.

CONCLUSIONS

The thermo–structural behavior of a series of fourteen $[Cu(cyclam)]_2[\{Cu(cyclam)\}_4\{(\alpha\text{–}GeW_{11}O_{39})Ln(H_2O)(OAc)\}_2]\cdot 18H_2O$ isostructural hybrid compounds (**1–Ln**, cyclam = 1,4,8,11–tetraazacyclotetradecane) has been analyzed in this work. The title compounds represent the first examples in which the $[\{(\alpha\text{–}XW_{11}O_{39})Ln(H_2O)(OAc)\}_2]^{n-}$ archetype is assembled through metalorganic linkers into a 2-dimensional covalent architecture. Our two synthetic methods have afforded derivatives in the form of single crystals for all Ln ions from La to Lu, thereby providing the first structural characterization of such archetype for Ln = La and Pr, as well as for the combinations of X = Ge with Ln = Ce, Nd, Sm or Lu.

Compounds **1–Ln** undergo two consecutive single-crystal-to-single-crystal transformations triggered by the thermal release of water molecules, which have been monitored by powder and single-crystal X-ray diffraction studies. Partial dehydration leads to the intermediate $[\{Cu(cyclam)\}_6\{(\alpha\text{–}GeW_{11}O_{39})Ln(H_2O)(OAc)\}_2]\cdot 4H_2O$ phase (**2–Ln**, determined for Ln = Eu and Er) through a process that involves formation and cleavage of Cu–O_{POM} bonds to result in the dimensionality of the parent framework being reduced from layers of bis-decorated polyoxotungstate dimers to chains in which such species are penta-decorated. Full release of water molecules leads to the $[Cu(cyclam)]_{0.5}[\{Cu(cyclam)\}_{5.5}\{(\alpha\text{–}GeW_{11}O_{39})Ln(OAc)\}_2]$ anhydrous phase (**3–Ln**, determined for Ln = Ce and Eu), in which the hybrid chains are essentially preserved but for the coexistence of tetra- and penta-decorated dimeric anions as a result of further disruption of Cu–O_{POM} bonds. Such **3–Ln** phases evidence for the first time that the aqua ligand coordinated to the Ln ions can be thermally evacuated to create coordinatively unsaturated derivatives of the $[\{(\alpha\text{–}XW_{11}O_{39})Ln(H_2O)(OAc)\}_2]^{n-}$ archetype without any significant skeletal affection. Both phase transitions have been found to be reversible, but with kinetics that depend on the Ln nature. The structure of **3–Ln** reverts back to the parent **1–Ln** framework simply upon short contact with ambient moisture for early-Ln-containing compounds (La to Sm), whereas immersion of crystal samples in water was required for achieving full structural reversion in the case of mid-to-late Ln-containing derivatives (Eu to Lu).

ASSOCIATED CONTENT

Supporting Information

The Supporting Information is available free of charge on the ACS Publications website at DOI: 10.1021/acs.inorgchem.0000000.
Experimental Section, FT–IR spectra, PXRD patterns, TGA/DTA curves, structural figures and tables (PDF).

Accession Codes

CCDC 1882845–1882858 (**1–Ln**, Ln = La to Lu), 1882862–1882863 (**2–Ln**, Ln = Eu, Er), 1882864–1882865 (**3–Ln**, Ln = Ce, Eu), and 1882859–1882861 (**1R–Ln**, Ln = Ce, Eu, Er) contain the supplementary crystallographic data for this paper. These data are provided free of charge by The Cambridge Crystallographic Data Centre.

AUTHOR INFORMATION

Corresponding Author

*E–mail: joseluis.vilas@ehu.es (J.L.V.)

*E–mail: juanma.zorrilla@ehu.es (J.M.G-Z)

ORCID

Beñat Artetxe: 0000-0002-7373-4596
Santiago Reinoso: 0000-0001-8329-5972
José Luis Vilas: 0000-0002-0188-4579
Juan M. Gutiérrez-Zorrilla: 0000-0001-8777-8533

Notes

The authors declare no competing financial interests.

ACKNOWLEDGMENT

This work was funded by Eusko Jaurlaritza/Gobierno Vasco (grant PIBA2018-59), MINECO (grant MAT2017-89553-P), and UPV/EHU (grants PPG17/37 and GIU17/050). S.R. thanks Obra Social la Caixa, Fundación Caja Navarra and UPNA for a research contract in the framework of the program "Captación del Talento". Technical and human support provided by SGIker (UPV/EHU) is gratefully acknowledged.

REFERENCES

(1) Halasz, I. Single-Crystal-to-Single-Crystal Reactivity: Gray, Rather than Black or White. *Cryst. Growth Des*. **2010**, *10*, 2817–2823.

(2) Ou, Y.-C.; Zhi, D.-S.; Liu, W.-T.; Ni, Z.-P.; Tong, M.-L. Single-Crystal-to-Single-Crystal Transformation from 1 D Staggered-Sculls Chains to 3 D NbO-Type Metal-Organic Framework through [2+2] Photodimerization. *Chem. Eur. J.* **2012**, *18*, 7357–7361.

(3) Wang, C.; Li, L.; Bell, J. G.; Lv, X.; Tang, S.; Zhao, X.; Thomas, K. M. Hysteretic Gas and Vapor Sorption in Flexible Interpenetrated Lanthanide-Based Metal–Organic Frameworks with Coordinated Molecular Gating via Reversible Single-Crystal-to-Single-Crystal Transformation for Enhanced Selectivity. *Chem. Mater.* **2015**, *27*, 1502–1516.

(4) Armentano, D.; De Munno, G.; Mastropietro, T. F.; Julve, M.; Lloret, F. Intermolecular Proton Transfer in Solid Phase: A Rare Example of Crystal-to-Crystal Transformation from Hydroxo- to Oxo-Bridged Iron(III) Molecule-Based Magnet. *J. Am. Chem. Soc.* **2005**, *127*, 10778–10779.

(5) Cheng, X.-N.; Zhang, W.-X.; Lin, Y.-Y.; Zheng, Y.-Z.; Chen, X.-M. A Dynamic Porous Magnet Exhibiting Reversible Guest-Induced Magnetic Behavior Modulation. *Adv. Mater.* **2007**, *19*, 1494–1498.

(6) Lv, G.-C.; Wang, P.; Liu, Q.; Fan, J.; Chen, K.; Sun, W.-Y. Unprecedented Crystal Dynamics: Reversible Cascades of Single-Crystal-to-Single-Crystal Transformations. *Chem. Commun.* **2012**, *48*, 10249–10251.

(7) Uchida, S.; Takahashi, E.; Mizuno, N. Porous Ionic Crystals Modified by Post-Synthesis of $K_2[Cr_3O(OOCH)_6(etpy)_3]_2[\alpha\text{-}SiW_{12}O_{40}]\cdot 8H_2O$ through Single-Crystal-to-Single-Crystal Transformation. *Inorg. Chem.* **2013**, 52, 9320–9326.

(8) Shi, L.-X.; Zhao, W.-F.; Xu, X.; Tang, J.; Wu, C.-D. From 1D to 3D Single-Crystal-to-Single-Crystal Structural Transformations Based on Linear Polyanion $[Mn_4(H_2O)_{18}WZnMn_2(H_2O)_2(ZnW_9O_{34})_2]^{4-}$. *Inorg. Chem.* **2011**, 50, 12387–12389.

(9) Campo, J.; Falvello, L. R.; Mayoral, I.; Palacio, F.; Soler, T.; Tomás, M. Reversible Single-Crystal-to-Single-Crystal Cross-Linking of a Ribbon of Cobalt Citrate Cubanes To Form a 2D Net. *J. Am. Chem. Soc.* **2008**, *130*, 2932–2933.

(10) Zhang, Y.-J.; Liu, T.; Kanegawa, S.; Sato, O. Reversible Single-Crystal-to-Single-Crystal Transformation from Achiral Antiferromagnetic Hexanuclears to a Chiral Ferrimagnetic Double Zigzag Chain. *J. Am. Chem. Soc.* **2009**, *131*, 7942–7943.

(11) Wriedt, M.; Yakovenko, A. A.; Halder, G. J.; Prosvirin, A. V.; Dunbar, K. R.; Zhou, H.-C. Reversible Switching from Antiferro- to Ferromagnetic Behavior by Solvent-Mediated, Thermally-Induced Phase Transitions in a Trimorphic MOF-Based Magnetic Sponge System. *J. Am. Chem. Soc.* **2013**, *135*, 4040–4050.

(12) Sarma, D.; Natarajan, S. Usefulness of in Situ Single Crystal to Single Crystal Transformation (SCSC) Studies in Understanding the Temperature-Dependent Dimensionality Cross-over and Structural Reorganization in Copper-Containing Metal–Organic Frameworks (MOFs). *Cryst. Growth Des.* **2011**, *11*, 5415–5423.

(13) Zhang, L.-Z.; Gu, W.; Liu, X.; Dong, Z.; Li, B. Solid-State Photopolymerization of a Photochromic Hybrid Based on Keggin Tungstophosphates. *CrystEngComm* **2008**, *10*, 652–654.

(14) Thiel, J.; Ritchie, C.; Streb, C.; Long, D.-L.; Cronin, L. Heteroatom-Controlled Kinetics of Switchable Polyoxometalate Frameworks. *J. Am. Chem. Soc.* **2009**, *131*, 4180–4181.

(15) Uehara, K.; Mizuno, N. Heterolytic Dissociation of Water Demonstrated by Crystal-to-Crystal Core Interconversion from (μ-Oxo)divanadium to Bis(μ-hydroxo)divanadium Substituted Polyoxometalates. *J. Am. Chem. Soc.* **2011**, *133*, 1622–1625.

(16) Friščić, T.; MacGillivray, L. R. Single-Crystal-to-Single-Crystal [2 + 2] Photodimerizations: From Discovery to Design. *Z. Kristallogr.* **2005**, *220*, 351–363.

(17) MacGillivray, L. R.; Papaefstathiou, G. S.; Friščić, T.; Hamilton, T. D.; Bučar, D.-K.; Chu, Q.; Varshney, D. B.; Georgiev, I. G. Supramolecular Control of Reactivity in the Solid State: From Templates to Ladderanes to Metal–Organic Frameworks. *Acc. Chem. Res.* **2008**, *41*, 280–291.

(18) Skoko, Z.; Zamir, S.; Naumov, P.; Bernstein, J. The Thermosalient Phenomenon. "Jumping Crystals" and Crystal Chemistry of the Anticholinergic Agent Oxitropium Bromide. *J. Am. Chem. Soc.* **2010**, *132*, 14191–14202.

(19) Bushuyev, O. S.; Tomberg, A.; Friščić, T.; Barrett, C. J. Shaping Crystals with Light: Crystal-to-Crystal Isomerization and Photomechanical Effect in Fluorinated Azobenzenes. *J. Am. Chem. Soc.* **2013**, *135*, 12556–12559.

(20) Hao, Z.-M.; Zhang, X.-M. Solvent Induced Molecular Magnetic Changes Observed in Single-Crystal-to-Single-Crystal Transformation. *Dalton Trans.* **2011**, *40*, 2092–2098.

(21) Vittal, J. J. Supramolecular Structural Transformations Involving Coordination Polymers in the Solid State. *Coord. Chem. Rev.* **2007**, *251*, 1781–1795.

(22) Coronado, E.; Mínguez Espallargas, G. Dynamic Magnetic MOFs. *Chem. Soc. Rev.* **2013**, *42*, 1525–1539.

(23) Ke, S.-Y.; Wang, C.-C. Water-Induced Reversible SCSC or Solid-State Structural Transformation in Coordination Polymers. *CrystEngComm* **2015**, *17*, 8776–8785.

(24) Vittal, J. J.; Quah, H. S. Photochemical Reactions of Metal Complexes in the Solid State. *Dalton Trans.* **2017**, *46*, 7120–7140.

(25) Vittal, J. J.; Quah, H. S. Engineering Solid State Structural Transformations of Metal Complexes. *Coord. Chem. Rev.* **2017**, *342*, 1–18.

(26) Reinoso, S.; Artetxe, B.; San Felices, L.; Gutiérrez-Zorrilla, J. M. Single-Crystal-to-Single-Crystal Transformations in Stimuli-Responsive Compounds Based on Polyoxometalate Clusters. In *Polyoxometalates. Properties, Structure and Synthesis*; Roberts, A. P., Ed.; Nova Science: Hauppauge, NY, USA, 2016; Chapter 6, pp 143–212.

(27) Fernández de Luis, R.; Urtiaga, M. K.; Mesa, J. L.; Orive Gómez de Segura, J.; Rojo, T.; Arriortua, M. I. $\{Co(HBpe)_2\}(V_4O_{12})$: Pedal Motion Induced Order–Disorder P–1 → C–1 Transition and Disrupted C–1 → C2/m Displacive Transition due to Thermal Instability. *CrystEngComm* **2011**, *13*, 6488-6498.

(28) Reinoso, S.; Dickman, M. H.; Praetorius, A.; Kortz, U. Low-Temperature Phase of Hexaguanidinium Heptamolybdate Monohydrate. *Acta Crystallogr., Sect. E* **2008**, *64*, m614-m615.

(29) Zhang, L.-Z.; Gu, W.; Dong, Z.; Liu, X.; Li, B. Phase Transformation of a Rare-Earth Anderson Polyoxometalate at Low Temperature. *CrystEngComm* **2008**, *10*, 1318–1320.

(30) Reinoso, S.; Artetxe, B.; Gutiérrez-Zorrilla, J. M. Single-Crystal-to-Single-Crystal Transformations Triggered by Dehydration in Polyoxometalate-Based Compounds. *Acta Crystallogr., Sect. C* **2018**, *74*, 1222–1242.

(31) Barats-Damatov, D.; Shimon, L. J. W.; Feldman, Y.; Bendikov, T.; Neumann, R. Solid-State Crystal-to-Crystal Phase Transitions and Reversible Structure–Temperature Behavior of Phosphovanadomolybdic Acid, $H_5PV_2Mo_{10}O_{40}$. *Inorg. Chem.* **2015**, *54*, 628–634.

(32) Chen, C.-L.; Goforth, A. M.; Smith, M. D.; Su, C.-Y.; zur Loye, H.-C. $[Co_2(ppca)_2(H_2O)(V_4O_{12})_{0.5}]$: A Framework Material Exhibiting Reversible Shrinkage and Expansion through a Single-Crystal-to-Single-Crystal Transformation Involving a Change in the Cobalt Coordination Environment. *Angew. Chem., Int. Ed.* **2005**, *44*, 6673–6677.

(33) Uchida, S.; Mizuno, N. Zeotype Ionic Crystal of $Cs_5[Cr_3O(OOCH)_6(H_2O)_3][\alpha\text{-}CoW_{12}O_{40}]\cdot 7.5H_2O$ with Shape-Selective Adsorption of Water. *J. Am. Chem. Soc.* **2004**, *126*, 1602–1603.

(34) Iturrospe, A.; Artetxe, B.; Reinoso, S.; San Felices, L.; Vitoria, P.; Lezama, L.; Gutiérrez-Zorrilla, J. M. Copper(II) Complexes of Tetradentate Pyridyl Ligands Supported on Keggin Polyoxometalates: Single-Crystal to Single-Crystal Transformations Promoted by Reversible Dehydration Processes. *Inorg. Chem.* **2013**, *52*, 3084–3093.

(35) Iturrospe, A.; San Felices, L.; Reinoso, S.; Artetxe, B.; Lezama, L.; Gutiérrez-Zorrilla, J. M. Reversible Dehydration in Polyoxometalate-Based Hybrid Compounds: A Study of Single-Crystal to Single-Crystal Transformations in Keggin-Type Germanotungstates Decorated with Copper(II) Complexes of Tetradentate N-Donor Ligands. *Cryst. Growth Des.* **2014**, *14*, 2318–2328.

(36) Pache, A.; Reinoso, S.; San Felices, L.; Iturrospe, A.; Lezama, L.; Gutiérrez-Zorrilla, J. M. Single-Crystal to Single-Crystal Reversible Transformations Induced by Thermal Dehydration in Keggin-Type Polyoxometalates Decorated with Copper(II)-Picolinate Complexes: The Structure Directing Role of Guanidinium. *Inorganics* **2015**, *3*, 194-218.

(37) Martín-Caballero, J.; Artetxe, B.; Reinoso, S.; San Felices, L.; Castillo, O.; Beobide, G.; Vilas, J. L.; Gutiérrez-Zorrilla, J. M. Thermally-Triggered Crystal Dynamics and Permanent Porosity in the First Heptatungstate-Metalorganic Three-Dimensional Hybrid Framework. *Chem. Eur. J.* **2017**, *23*, 14962-14974.

(38) Martín-Caballero, J.; Wéry, A. S. J.; Artetxe, B.; Reinoso, S.; San Felices, L.; Vilas, J. L.; Gutiérrez-Zorrilla, J. M. Sequential Single-Crystal-to-Single-Crystal Transformations Promoted by Gradual Thermal Dehydration in a Porous Metavanadate Hybrid *CrystEngComm* **2015**, *17*, 8915–8925.

(39) Martín-Caballero, J.; Wéry, A. S. J.; Reinoso, S.; Artetxe, B.; San Felices, L.; El Bakkali, B.; Trautwein, G.; Alcañiz-Monge, J.; Vilas, J. L.; Gutiérrez-Zorrilla, J. M. A Robust Open Framework Formed by Decavanadate Clusters and Copper(II) Complexes of Macrocyclic Polyamines: Permanent Microporosity and Catalytic Oxidation of Cycloalkanes. *Inorg. Chem.* **2016**, *55*, 4970–4979.

(40) Dissem, N.; Artetxe, B.; San Felices, L.; Lezama, L.; Haddad, A.; Gutiérrez-Zorrilla, J. M. A Robust Framework Based on Polymeric Octamolybdate Anions and Copper(II) Complexes of Tetradentate N-donor Ligands. *Crystals* **2018**, *8*, 20.

(41) Pope, M. T. *Heteropoly and Isopoly Oxometalates*; Springer: Berlin, 1983.

(42) *Polyoxometalate Chemistry. Some Recent Trends*; Sécheresse, F., Ed.; World Scientific: Singapore, 2013.

(43) Ma, X.; Yang, W.; Chen, L.; Zhao, J. Significant Developments in Rare-Earth-Containing Polyoxometalate Chemistry: Synthetic Strategies, Structural Diversities and Correlative Properties. *CrystEngComm* **2015**, *17*, 8175-8197.

(44) Boskovic C. Rare Earth Polyoxometalates. *Acc. Chem. Res.* **2017**, *50*, 2205-2214.

(45) Mialane, P.; Dolbecq, A.; Rivière, E.; Marrot, J.; Sècheresse, F. Functionalization of Polyoxometalates by a Negatively Charged Bridging Ligand: The Dimeric $[(SiW_{11}O_{39}Ln)_2(\mu\text{-}CH_3COO)_2]^{12-}$ (Ln = Gd^{III}, Yb^{III}) Complexes. *Eur. J. Inorg. Chem.* **2004**, 33–36.

(46) Hussain, F.; Sandriesser, S.; Speldrich, M.; Patzke, G. R. A New Series of Lanthanoid Containing Keggin-Type Germanotungstates with Acetate Chelators: $[\{Ln(CH_3COO)GeW_{11}O_{39}(H_2O)\}_2]^{12-}$ {*Ln*=Eu^{III}, Gd^{III}, Tb^{III}, Dy^{III}, Ho^{III}, Er^{III}, Tm^{III}, and Yb^{III}}. *J. Solid State Chem.* **2011**, *184*, 214–219.

(47) Niu, J.; Wang, K.; Chen, H.; Zhao, J.; Ma, P.; Wang, J.; Li, M.; Bai, Y.; Dang, D. Assembly Chemistry between Lanthanide Cations and Monovacant Keggin Polyoxotungstates: Two Types of Lanthanide Substituted Phosphotungstates $[\{(\alpha\text{-}PW_{11}O_{39}H)Ln(H_2O)_3\}_2]^{6-}$ and $[\{(\alpha\text{-}PW_{11}O_{39})Ln(H_2O)(\eta^2,\mu\text{-}1,1)\text{-}CH_3COO\}_2]^{10-}$. *Cryst. Growth Des.* **2009,** *9*, 4362–4372.

(48) Saini, M. K.; Gupta, R.; Parbhakar, S.; Mishra, A. K.; Mathur, R.; Hussain, F. Dimeric Complexes of Rare-Earth Substituted Keggin-Type Silicotungstates: Syntheses, Crystal Structure and Solid State Properties. *RSC Adv.* **2014**, 4, 25357–25364.

(49) Zhang, D.; Zhang, C.; Chen, H.; Ma, P.; Wang, J.; Niu, J. Syntheses, Structures and Properties of Dimeric Rare Earth Derivatives Based on Monovacant Keggin-Type Polyoxotungstates. *Inorg. Chim. Acta* **2012**, *391*, 218–223.

(50) Du, D.; Qin, J.; Li, S.; Lan, Y.; Wang, X.; Su, Z. 3d–4f Heterometallic Complexes for the Construction of POM-Based Inorganic–Organic Hybrid Compounds: from Nanoclusters to One-Dimensional Ladder-Like Chains. *Aust. J. Chem.* **2010**, *63*, 1389–1395.

(51) Zhao, H.-Y.; Zhao, J.-W.; Yang, B.-F.; He, H.; Yang, G.-Y. Organic–Inorganic Hybrids Based on Monovacant Keggin-Type Polyoxotungstates and 3d–4f Heterometals. *CrystEngComm* **2013**, *15*, 8186–8194.

(52) Kehl, W. L.; Hay, R. G.; Wahl, D. The Structure of Tetragonal Tungsten Trioxide. *J. Appl. Phys.* **1952**, *23*, 212–215.

(53) Schofield, P. F.; Knight, K. S.; Redfern, S. A. T.; Cressey, G. Distortion Characteristics Across the Structural Phase Transition in $(Cu_{1-x}Zn_x)WO_4$. *Acta Crystallogr., Sect. B.* **1997**, 53, 102–112.

(54) Forsyth, J. B.; Wilkinson, C.; Zvyagin, A. I. The Antiferromagnetic Structure of Copper Tungstate, $CuWO_4$. *J. Phys.: Condens. Matter* **1991**, *3*, 8433–8440.

(55) Klein, S.; Weitzel, H. PERNOD - Ein Programm zur Verfeinerung von Kristallstrukturparametern aus Neutronenbeugungspulverdiagrammen. *J. Appl. Crystallogr.* **1975,** *8*, 54–59.

(56) Pestereva, N.; Guseva, A.; Vyatkin, I.; Lopatin, D. Electrotransport in Tungstates $Ln_2(WO_4)_3$ (Ln = La, Sm, Eu, Gd). *Solid State Ionics* **2017**, *301*, 72–77.

(57) Artetxe, B.; Reinoso, S.; San Felices, L.; Lezama, L.; Gutiérrez-Zorrilla, J. M.; García, J. A.; Galán-Mascarós, J. R.; Haider, A.; Kortz, U.; Vicent, C. Cation-Directed Dimeric versus Tetrameric Assemblies of Lanthanide-Stabilized Dilacunary Keggin Tungstogermanates. *Chem. Eur. J.* **2014**, *20*, 12144–12156.

(58) Bassil, B. S.; Dickman, M. H.; von der Kammer, B.; Kortz, U. The Monolanthanide-Containing Silicotungstates $[Ln(\beta_2\text{-}SiW_{11}O_{39})_2]^{13-}$ (Ln = La, Ce, Sm, Eu, Gd, Tb, Yb, Lu): A Synthetic and Structural Investigation. *Inorg. Chem.* **2007**, *46*, 2452–2458.

(59) Casanova, D.; Llunell, M.; Alemany,P.; Alvarez, S. The Rich Stereochemistry of Eight-Vertex Polyhedra: A Continuous Shape Measures Study. *Chem. Eur. J.* **2005**, *11*, 1479–1494.

(60) Bosnich, B.; Poon, C. K.; Tobe, M. L. Complexes of Cobalt(III) with a Cyclic Tetradentate Secondary Amine. *Inorg. Chem.* **1965**, *4*, 1102–1108.

(61) Bakaj, M.; Zimmer, M. Conformational Analysis of Copper(II) 1,4,8,11-Tetraazacyclotetradecane Macrocyclic Systems. *J. Mol. Struct.* **1999**, *508*, 59–72.

(62) Spek, A. L. Structure Validation in Chemical Crystallography. *Acta Crystallogr.* **2009**, *D65*, 148–155.

SYNOPSIS TOC.

Thermal dehydration of the first 2-dimensional covalent hybrid lattice based on $[(\alpha\text{–}XW_{11}O_{39})Ln(H_2O)(OAc)\}_2]^{12-}$ polyoxometalates (**1–Ln,** Ln = La–Lu) proceeds via two sequential single–crystal–to–single–crystal transformations that result in 1-dimensional covalent assemblies for the intermediate **2–Ln** and anhydrous **3–Ln** phases upon modifications in the Cu–O_{POM} bonding scheme. The La-to-Sm-containing compounds revert back to the **1–Ln** framework upon air exposure whereas Eu-to-Lu-containing analogues require immersion in water.